WATER DROPS AND CAVITATION BUBBLES IN MICROGRAVITY

P. Kobel[1*], D. Obreschkow[1†], N. Dorsaz[1], A. de Bosset[1], C. Nicollier[2], and M. Farhat[1]

[1] *École Polytechnique Fédérale de Lausanne (EPFL)*
CH-1015 Lausanne, Switzerland

[2] *ESA European Astronaut Centre, Cologne, Germany,*
and NASA Johnson Space Center, Houston, TX

(Dated: April 9, 2006)

We realized an experimental setup to study the dynamics of cavitation bubbles inside spherical water drops produced in microgravity (8th Student Parabolic Flight Campaign, European Space Agency ESA). Water volumes of up to 8 ml (25 mm diameter) were expelled through a specially designed *injector tube*. The latter contained a porous hydrophilic foam and was particularly coated to ensure a stable and attached water drop. Single cavitation bubbles were then generated by an electrical discharge inside the drop. The growth and collapse of the bubble were recorded using a high-speed visualization system (24'000 frames/s). Thereby, we could study for the first time the cavitation phenomenon in microgravity and observe the interactions between cavity and spherical free surface. In particular, the microjet/counterjet formation was visualized and significant counterjet broadening was found when passing from planar to spherical free surfaces.

I. INTRODUCTION

The hydrodynamic cavitation phenomenon is of prime importance for many industrial systems, [1], such as cryogenic pumps for rocket propulsion, fast ship propellers and hydraulic turbines. It occurs in a large variety of liquids, e.g. water, glycerine [2] or mercury [3], and may cause strong vibrations, serious efficiency loss and erosion damage. Motivated by the vision to realize design changes or surface coatings preventing from such damages, cavitation has become an important research topic in fluid engineering. A major subject within this research is the violent collapse of cavity bubbles, which usually generates liquid jets [4], shockwaves [5] and luminescence [6].

The behavior of cavitation bubbles is known to be strongly dependent on the nature of nearby boundaries, since the latter dictate the distribution of the surrounding pressure field [7]. Recent studies of bubbles collapsing beneath a planar free surface revealed the existence of fast liquid jets directed inside the liquid (*microjets*) and slow liquid spikes escaping from the liquid (*counterjets*). However, the dynamics of bubbles next to *spherical* free surfaces has never been observed due to the difficulty of creating such surfaces in the presence of gravity. This is nevertheless an important issue since curved surfaces appear dynamically in water flows, and the bubble motion is significantly dependent on the surface curvature, as shown in the case of *rigid* curved boundaries [8]. Thus, the study of cavitation next to curved free surfaces is a promising tool for novel insight in interactions between bubbles and free surface.

In the present study, we intended to investigate the dynamics of a cavitation bubble inside a spherical water drop, with particular focus on the interaction between cavity and spherical free surface. For this purpose, the dynamics of a spark-generated bubble was observed inside a liquid drop realized under microgravity conditions. A specific instrumentation has been developed to ensure the creation of large stable water drops as well as the high speed flow visualization by taking into account the requirements of microgravity flights. The bubble's radius and its location inside the drop have been varied. The experiment was carried out in zero-g parabolic flights during the 8th ESA's Student Parabolic Flight Campaign.

II. FLIGHT MANEUVER

The microgravity maneuvers are flown with the "Airbus A300 zero-g", a specially equipped aircraft owned by NOVESPACE and hosted at the military airport Merignac in France.

From a steady horizontal flight, the aircraft gradually pulls up its nose and ends climbing at an angle of approximately 47 degrees. This preparatory phase lasts for about 20 seconds, during which the aircraft experiences an acceleration of around 1.8 g, oriented perpendicularly to the aircraft's plane. The engine thrust is then suddenly reduced to the minimum required to compensate for air-drag, and the aircraft

* philippe.kobel@a3.epfl.ch
† danail.obreschkow@spacescience.ch

follows a free-fall ballistic trajectory, i.e. a parabola, lasting for approximately 20 seconds, during which weightlessness is achieved. At the end of this period, the aircraft must pull out of the parabolic arc, a maneuver which gives rise to another 20 second period of 1.8 g. Finally it returns to a steady horizontal flight.

These maneuvers are flown repeatedly, with a period of 3 minutes between the start of two consecutive parabolas, i.e. a 1 minute parabolic phase (20 seconds at 1.8 g, 20 seconds of weightlessness, 20 seconds at 1.8 g), followed by a 2 minute "rest" period at 1 g. After parabolas 5, 10, 15, 20 and 25, the rest interval is increased to 6 or 8 minutes.

III. EXPERIMENTAL CYCLE AND SETUP

The experimental procedure is designed to perform *one* experimental cycle (i.e. water drop formation, cavitation bubble generation and subsequent dynamics) per parabola. More precisely, a spherical water drop having a radius from 8 mm to 13 mm (2.5 ml to 8 ml) is smoothly expelled over 5 s to 15 s. Thereafter, the cavity is generated through an electrical discharge. It grows, collapses and rebounds in a few milliseconds (!). The slow drop growth and the fast cavitation process are recorded using a standard video-camera and a high speed ccd-camera, respectively.

A schematized overview of the main components is given in Fig. 1. The water drop is generated inside a transparent and sealed cubic vessel made of Lexan. The standard camera (Sony Camcorder, 25 f/s, 768×576 pixel) and the fast camera (Photron Ultima APX, up to 120'000 f/s, 1024×1024 pixel) are placed on the same optical axis and oriented in opposite directions. Whereas the standard camera films the whole experiment, the fast camera only records a short interval (11 ms) covering the cavity life-cycle. During this short sequence, a perpendicularly placed high power flashlight (Cordin Light Source Model 359) releases a single flash having 11 ms duration.

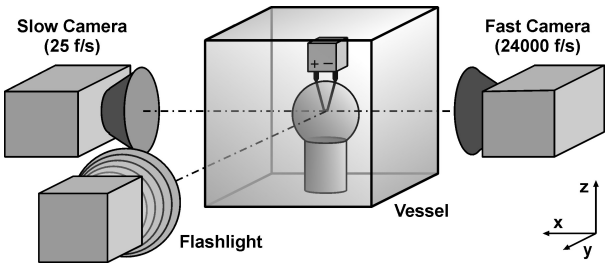

FIG. 1: Cameras and flashlight disposition around the vessel containing the injector tube and the electrodes.

Inside the transparent vessel, the water drop is smoothly expelled through a custom-designed aluminum *injector tube* with the help of a programmable micro-pump. The pumping flux is set to 0.6 ml/s and reduced to 0.3 ml/s during the last two seconds of the pumping process, in order to slow down the drops motion. By virtue of surface tension, the water volume naturally forms a truncated spherical drop (see Fig. 2 left). The tube is filled with hydrophilic porous foam that guaranties a homogeneous laminar water flow, damps out eventual oscillations and favors the attachment of the water drop. To further ensure the attachment of the drop, the top edge is drilled at an angle of 45° with respect to the horizontal, allowing a truncated spherical water drop of 2.5 ml volume to sit on the tube with continuous surface curvature at the attachment point (Fig. 2 left). In addition, the inclined top edge is coated with hydrophilic aluminum oxide Al_2O_3. The tube outside is coated with a hydrophobic silicon layer to prevent the water from flowing down along the tube.

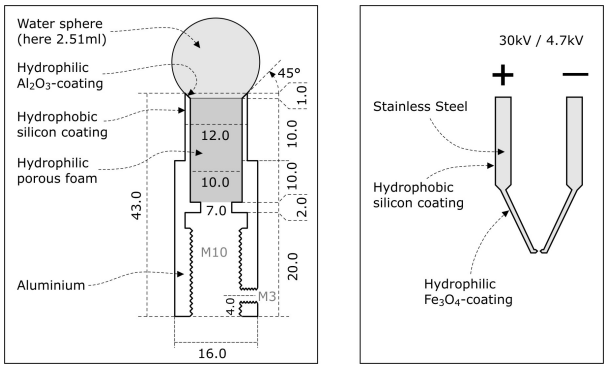

FIG. 2: Left: injector tube with water drop. Right: electrodes for bubble generation.

The cavitation bubbles are generated trough an electrical discharge between two electrodes immersed in the water drop. Using micro-controllers, the electrodes position within the drop can be precisely varied in the three space dimensions. To minimize distortion of the drop by the electrodes, their tips are coated with hydrophilic ferrous oxide Fe_3O_4 and their upper part is covered with hydrophobic paraffine (Fig. 2 right). The high voltage between the electrodes (40 kV) leads to the formation of a plasma that allows the fast discharge of a previously charged capacitor with a capacitance of either 30 nF or 200 nF (charged at 4.3 kV). Shortly after this discharge, the plasma recombines, forming a volume of superheated water vapor that grows as a bubble (see [9] for more details). Discharge-induced cavities were chosen instead of laser-induced ones, because of the difficulty to focus a laser beam across a (variable) spherical surface and for aircraft security reasons.

The gravity level is monitored by an accelerometer (Memsic, 2125 Dual-axis Accelerometer), which is used to trigger the experiment. It provides the starting signal when the gravity level falls below 0.2 g for more than 1 s. Immediately after the water drop formation, the electrical discharge for cavity generation triggers simultaneously the high-speed camera and the flash light through an inductive circuit. Once the microgravity phase is over, the water sphere is naturally removed by hypergravity and absorbed by sponges covering the vessel bottom. The temporal sequence containing the g-sensor data, micro-pump flux and instant of discharge release is controlled by a Notebook, which also records the high-speed camera data.

IV. RESULTS

In this paragraph we present and discuss the results obtained during two parabolic flight days with 30 parabolas each. Three physical parameters were sequentially varied: (1) the water drop volume, (2) the cavitation bubble size and (3) its position.

A. Water Drop in Microgravity

Most experiments revealed that water drops with a diameter of up to 25 mm (8 ml volume) were stable and conveniently attached to the injector tube during the whole microgravity phase (see Fig. 3). We conclude that the implemented injector tube was adequately designed to generate and stabilize a spherical water drop in microgravity.

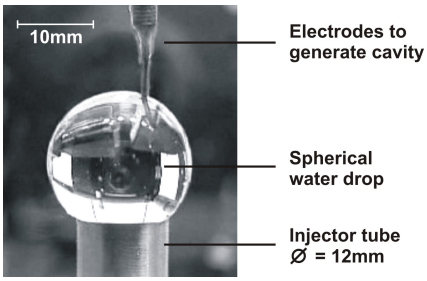

FIG. 3: Stable spherical water drop on injector tube during weightlessness.

In 10% of the zero-g parabolas, we recorded flight-based deviations from the zero-g level larger than 0.05 g for durations longer than 0.2 s. They mostly occurred towards the end of the zero-g cycle, approximately 3 s before the "pull out" command, which terminates the parabola. The injector tube being fixed to the aircraft reference, those fluctuations induced observable oscillations of the water drop, such as shown in Fig. 4. However, such oscillations damp out rapidly within characteristic times of 0.5 s to 1 s. We argue that the large area of support attaching the drop to the tube (1.1 cm^2) is responsible for this efficient attenuation, since the large porous foam ensures an inelastic rebound of the water drop.

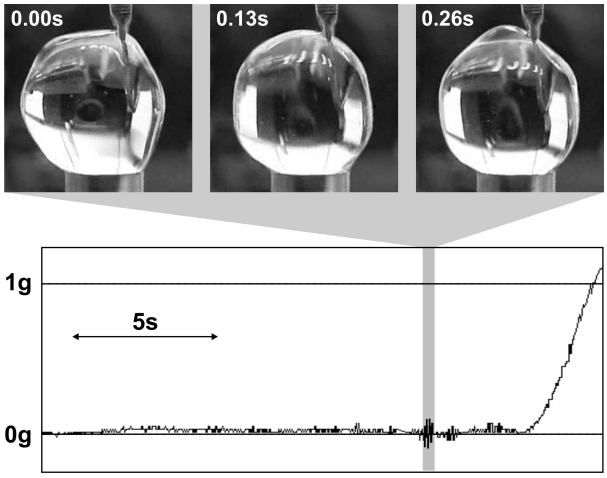

FIG. 4: Water drop oscillations resulting from zero gravity imperfections.

Despite of the careful electrode preparation, we observed significant water sphere distortion by electrode-water interaction. During the first flight day, the upper part of the electrodes (thick part) was too hydrophilic yielding oblong distortion of the water volume. Conversely, additional paraffine coverage engendered water repulsion by the electrodes during the initial phase of the second flight day. Digital camera images of ideal spherical, attracted oblong, and repulsed water drops are shown in Fig. 5. Because of this distortion, the electrodes were readjusted during the flight to assure the controlled emission of liquid jets (section IV B). Moreover, the drops deviations from a perfect sphere render the definition of quantitative parameters such as the curvature ratio between drop and cavity more complex. Hence, comparisons to theoretical models become harder. This reveals the necessity to optimize the electrodes surface coating and to render the tips finer to minimize possible interactions.

FIG. 5: Left: ideal spherical drop (3.5 ml), Center: attracted oblong drop (7 ml), Right: repulsed drop (5 ml).

B. Cavitation Bubbles in Microgravity

We first describe the global aspects of an entire cavitation bubble cycle, consisting in bubble growth, collapse and jet emission. Fig. 6 shows the important steps of such a cycle, starting with the release of an electrical discharge, with an energy of about 0.3 Joules (case of 30 nF). The process was filmed at 24'000 frames/sec (41.67 μs between subsequent images), each frame being exposed for 4 μs in order to achieve maximum sharpness.

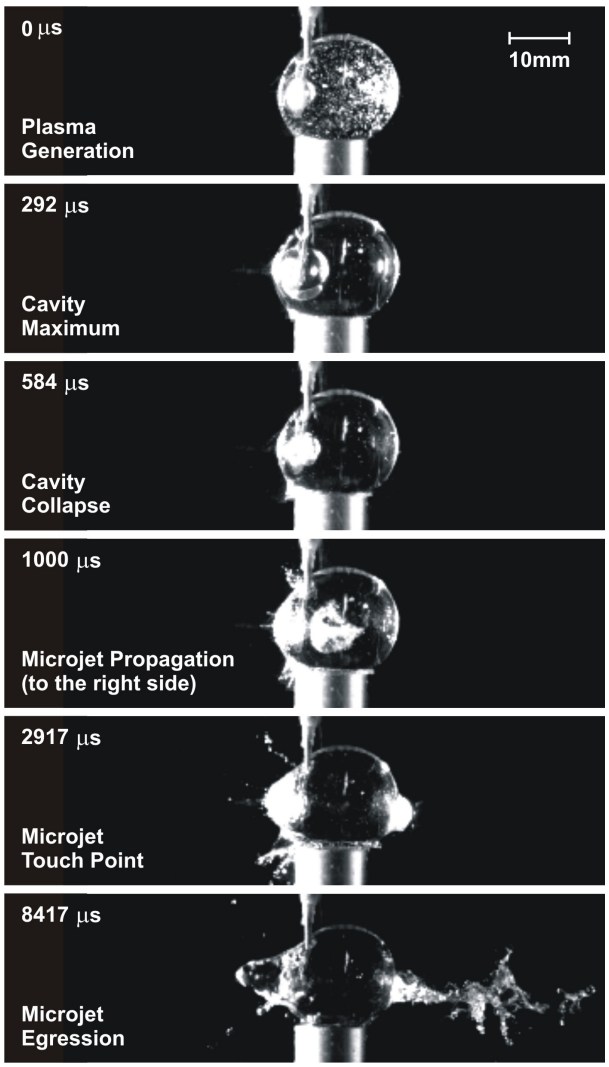

FIG. 6: Entire cycle from cavity generation to liquid jet escape.

Qualitatively, this series compares to our expectations from ground-based experiments (e.g. [10], [11]), basic theory (Rayleigh-Plesset) and numerical simulations (e.g. [12]): The discharge-induced bubble evolves temporally symmetrically, its growth time and collapse time being identical (192 μs) up to the frame rate precision. Since the bubble collapses close to a free surface, it looses its spherical symmetry in the course of the implosion (*toroidal implosion*). Thereby, it ejects two liquid jets perpendicularly to the closest surface element – the fast *microjet* (towards the right side) and the slower *counterjet* (towards the left side). The microjet accelerates the surrounding water regime to an average recoil speed of 10.2±0.5 m/s. It then reaches the opposite drop surface and escapes at a reduced velocity of 5.8±0.5 m/s.

To the best of our knowledge, this microgravity experiment allowed for the first time the observation of the entire microjet-counterjet pair escaping from a *stationary* liquid regime. Comparatively, recent ground-based experiments with cavitation bubbles inside a cylinder-like water stream showed similar microjets that were distorted due to the relative motion of the water regime [3].

We shall now have a close look at the counterjet geometry. It significantly differs from our expectations based on ground experiments. Indeed, the counterjet coming out of the spherical water drop is hardly pointed and resembles rather a droplet, whereas similar jets on ground-based planar surfaces are very peaked (see Fig. 7).

FIG. 7: Left: Counterjet on a spherical free surface in micro-gravity (electrodes enter from the right). Right: Counterjet on a planar free surface on ground.

For flat free surfaces, the narrow liquid jet was shown to result from a highly localized pressure peak between cavity boundary and free surface (see numerical simulations [12]). A qualitative attempt to explain the different behavior of our microgravity experiment uses the *sphericity* of the drops. The *concave curvature* of the free surface leads to a smooth variation of the distance between cavity boundary and free surface. Therefore, the cavity "feels" the proximity of a *vast* region of the free surface. Differently speaking, the pressure peak in between cavity and spherical free surface occupies a larger region. Since this pressure peak forms the basis of the counterjet, the latter becomes broader. This explanation is compatible with recent studies of interactions between bubbles and *rigid* curved surfaces [8].

V. CONCLUSION

The experiment reported here has been the first study of the cavitation phenomenon in microgravity. Its main goal was to study the interaction of cavitation bubbles with spherical free surfaces.

Stable water volumes of up to 8 ml were produced and remained attached to the injector tube during the complete microgravity phase, thereby showing the adequate design of the injector tube. Initially encountered difficulties to create spherical water drops (due to electrodes-water attraction/repulsion) were carefully investigated. These studies clearly showed the necessity of using electrodes with large tips and suitable surface coating.

To the best of our knowledge, this experiment allowed for the first time the observation of the whole microjet-counterjet pair escaping from a *stationary* regime of water. Those images are an adequate visualization of theories and numerical results about toroidal implosion. A striking result in this respect was a significant counterjet broadening relative to ground-based studies. We attribute this phenomenon to both the free surfaces sphericity.

Based on those scientific results, this experiment may be considered a proof-of-principle of cavitation research in microgravity. For the future, we propose an enhanced version of the experiment with (1) an optimized electrode design/coating, (2) a higher optical resolution and (3) a broader range of discharge capacitances. These improvements are necessary in order to investigate more systematically the influence of the free surface curvature on the cavitation bubble dynamics with a particular emphasis on the discovered counterjet broadening.

VI. ACKNOWLEDGEMENTS

We gratefully acknowledge the *European Space Agency (ESA)* for having offered the possibility to pursue these experiments on parabolic flights. Furthermore, our gratitude is directed to the *Swiss National Science Foundation (SNSF)* who provided the substantial basis of the whole research frame. We also thank several institutions of the *École Polytechnique Fédérale de Lausanne (EPFL)* for their support in financial, practical and theoretical aspects. Finally, we thank our private donator, the *Swiss Space Industry Group (SSIG)*.

[1] Avellan F. "Cavitation in Hydraulic Turbines" Keynote Lecture, 5th International Symposium on Cavitation CAV2003, Osaka, Japan. 2003.

[2] Frost D, Sturtevant B. Journal of Heat Transfer-Transactions of the ASME 108 (2): 418-424. May 1986.

[3] Robert E, Master Thesis EPFL LMH. 2004.

[4] Escaler X, Dupont P, Avellan F. "Experimental investigation on forces due to vortex cavitation collapse for different materials." Wear 233(12): 65-74. 1999.

[5] Guennoun F, Farhat M, Ait Bouziad Y, Avellan F, Pereira F. "Experimental Investigation of a Particular Traveling Bubble Cavitation ". Proceedings of the 5th International Symposium on Cavitation CAV2003, Osaka, Japan. 2003.

[6] Lettry J, Fabich A, Gilardoni S, Benedikt M, Farhat M, Robert E. "Thermal shocks and magnetohydrodynamics in high power mercury jet targets". Journal of Physics G: Nuclear and Particle Physics 29(8): 1621-1627. 2003.

[7] Gibson DC, Blake JR. Applied Scientific Research 38: 215-224. 1982.

[8] Tomita Y, Robinson PB, Tong RP, Blake JR. Journal of Fluid Mechanics 466: 259-283. Sept 2002.

[9] Pereira F, Farhat M, Avellan F. "Dynamic calibration of transient sensors by spark generated cavity" in "Bubble Dynamics and Interface Phenomena", 227-240. J.R. Blake et al. (eds.). 1994.

[10] Benjamin TB, Ellis AT. Philosophical Transactions of the Royal Society of London. Series A-Mathematical and Physical Sciences 260 (1110): 221-&. 1966.

[11] Crum LA, Journal de Physique 41: 285-288 Suppl. 8, 1979.

[12] Robinson PB, Blake JR, Kodama T, Shima A, Tomita Y. Journal of Applied Physics 89 (12): 8225-8237. Jun 2001.